Investigations of the synthesis of the superheavy element $Z = 122$

H. C. Manjunatha,[1,*] K. N. Sridhar,[2,3] and N. Sowmya[1]

[1]*Department of Physics, Government College for Women, Kolar-563101 Karnataka, India*
[2]*Department of Physics, Government First Grade College, Kolar-563101 Karnataka, India*
[3]*Research and Development Centre, Bharathiar University, Coimbatore-641046, India*

(Received 18 May 2018; published 15 August 2018)

We have identified the most probable projectile-target combination by studying the fusion cross section, evaporation residue cross section, compound nucleus formation probability (P_{CN}), and survival probability (P_{Surv}) of different projectile target combinations to synthesize the superheavy element $Z = 122$. The selected most probable projectile-target combinations to synthesize the superheavy element $Z = 122$ are Cr + Cf, Fe + Cm, Se + Ra, and As + Ac. Superheavy nuclei may decay through the different decay modes such as spontaneous fission, ternary fission, and cluster decay. We have also studied the half-lives of spontaneous fission, ternary fission, and cluster decay of the predicted nuclei for $Z = 122$ and compared with that of alpha decay. This enables us to study the competition between spontaneous fission, ternary fission, cluster decay, and alpha decay in the superheavy nuclei of $Z = 122$. The comparision of half lives for different decay modes reveals that alpha decay is having smaller half lives than the other studied decay modes. A detail study of branching ratio of alpha decay with respect to other decay modes also confirms that alpha decay is most dominant decay mode for the isotopes superheavy nuclei $^{307-314}122$ and hence these nuclei can be detected through the alpha decay mode only. We hope that our predictions may be guide for the future experiments in the synthesis of more isotopes of superheavy nuclei Z = 122.

DOI: 10.1103/PhysRevC.98.024308

I. INTRODUCTION

The study of superheavy elements has become the subject of strong interest both for experimental and theoretical research. Superheavy elements are formed by a fusion process in collisions of two heavy ions. The fusion is described in the literature with two different methods: as a melting of two nuclei along their relative coordinate or as a transfer of nucleons or clusters from the lighter nucleus to the heavier one. In this paper we describe the fusion as a melting process along the relative coordinate. The other method is based on the dinuclear system (DNS) concept (see Refs. [1,2]). In this model the formed DNS evolves as a diffusion process in the mass asymmetry coordinate $\eta = (A1 - A2)/(A1 + A2)$ to the compound nucleus. The DNS model assumes that the motion to smaller relative distances (at fixed η) is hindered in collisions of heavy nuclei [3]. The diffusion process can lead to the decay of the dinuclear system, which is quasifission. Torres *et al.* [4] studied the quasifission process in a transport model for a dinuclear system. The competition between fusion and quasifission reduces the cross section for the compound nucleus formation. The DNS model works well for the description of fusion in symmetric reactions with heavy nuclei and in reactions producing superheavy nuclei [5]. The dependence of the fusion cross section on the isotopic composition of colliding nuclei is studied using the dinuclear system concept for compound nucleus formation [6]. Adamian *et al.* [7] studied the possibilities of the synthesis of superheavy nuclei in actinide based fusion reactions within the dinuclear system model for compound nucleus formation. Previous workers studied the influence of angular momentum on the competition between complete fusion and quasifission within the dinuclear system model [8]. The use of light- and medium-mass neutron-rich radioactive beams may produce superheavy nuclei. Such a possibility is also provided by the multinucleon transfer processes in low-energy damped collisions of heavy actinide nuclei, if the shell effects really play an important role in such reactions [9]. Multinucleon transfer reactions occurring in low-energy collisions of heavy ions are considered an important method for the production of superheavy elements [10]. The possibilities of using radioactive beams, multinucleon transfer reactions, and neutron capture processes for this purpose are discussed by previous workers [11–13]. Marinov *et al.* [14] obtained possible evidence for the existence of a long-lived superheavy nucleus with mass number $A = 292$ and atomic number $Z = 122$ or 124 in natural thorium. The discovery of many isotopes of new superheavy elements of $Z = 114$, 115, 116, 118 were reported in a review paper [15]. There have been some experimental studies reported on the investigations of superheavy nuclei (SHN) $Z = 122$ [16,17]. Some theoretical studies also observed on the predictions of SHN $Z = 122$ [18–20]. Previous theoretical studies on the evaporation residue (σ_{ER}) cross section for $Z = 122$ refer to a cold, near-symmetric reaction $^{154}\mathrm{Sm}(^{150}\mathrm{Nd},\ 1n)^{303}122$ [18,19]. Also observed is the synthesis of the superheavy element $Z = 122$ through a hot fusion reaction ($^{58}\mathrm{Fe} + {}^{248}\mathrm{Cm} \rightarrow {}^{306-x}122 + xn$ and $^{64}\mathrm{Ni} + {}^{244}\mathrm{Pu} \rightarrow {}^{308-x}122 + xn$) [20].

*Corresponding author: manjunathhc@rediffmail.com

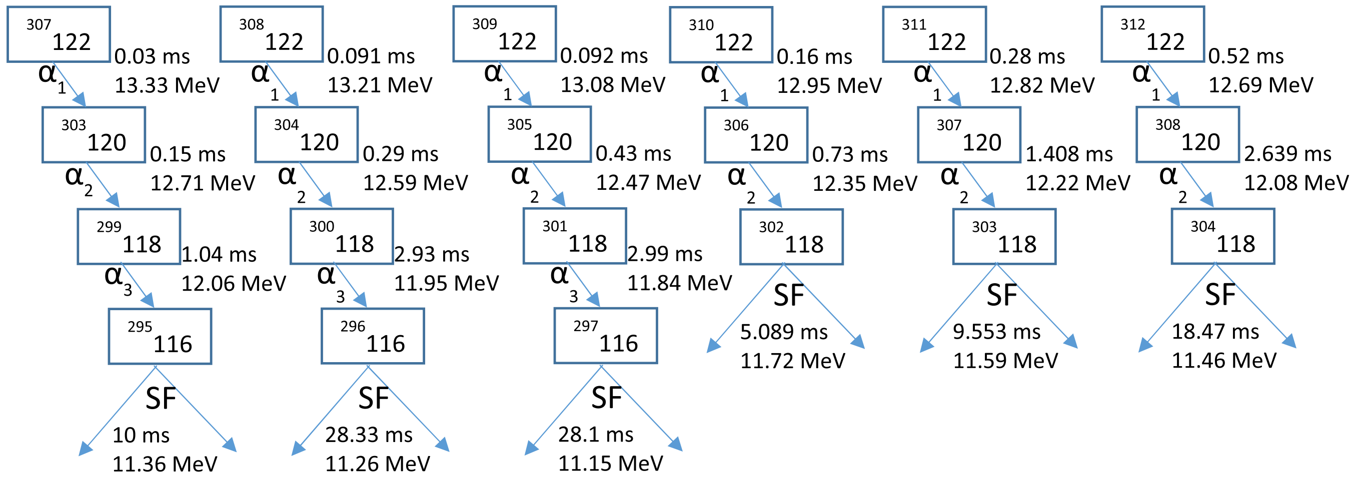

FIG. 1. Decay chain of the predicted probable isotopes for $Z = 122$.

The predicted value of the $1n$ decay cross section for the cold fusion reaction ^{154}Sm(^{150}Nd, $1n$)^{303}122 by previous researchers [16] using the fusion-by-diffusion (FBD) model [21–23] is $\sigma_{1n} \sim 10^{-11}$ pb, whereas other authors [17] had predicted the same to be ~1 pb, an incredible 11 orders of magnitude higher, for their use of an old variant of the FBD model [21]. There is a discrepancy in the predictions of synthesis parameters of superheavy nuclei. The hot fusion reactions have been used as the tool to study the SHEs. Superheavy nuclei and their decay properties is one of the important fields in nuclear physics. Previous researchers [14] obtained the half-life $T_{1/2} > 10^8$ yr and an abundance $(1-10) \times 10^{-12}$ for a superheavy nucleus with mass number $A = 292$ and atomic number $Z = 122$. The possibility of such an extremely heavy Z nucleus motivated us to study the most probable projectile-target combinations to synthesize the superheavy nuclei $Z = 122$. Previous researchers also studied the possible projectile target combinations to synthesize the superheavy nuclei [22–28].

Manjunatha [26] studied the theoretical predictions on the possible isotopes of the superheavy element $Z = 122$ and predicted that the nuclei $^{307-314}$122 were found to have long half-lives and hence could be sufficient to detect them if synthesized in a laboratory. The decay chains of predicted nuclei for $Z = 122$ are shown in Fig. 1. The present work consists of two parts. In the first part we have identified the most probable projectile-target combination to synthesize these superheavy nuclei. We have identified the most probable projectile-target combination by studying the fusion cross section, evaporation residue cross section, compound nucleus formation probability (P_{CN}), and survival probability (P_{Surv}) of different projectile target combinations to synthesize the superheavy element $Z = 122$. Superheavy nuclei may decay through the different decay modes such as spontaneous fission, ternary fission, and cluster decay. There is a need to study the different decay modes such as spontaneous fission, ternary fission, and cluster decay of the predicted nuclei for $Z = 122$. Hence in the second part of this work, we have studied the half-lives of spontaneous fission, ternary fission, and cluster decay of this predicted nuclei for $Z = 122$ and compared them with that of alpha decay. This enables us to study the competition between spontaneous fission, ternary fission, cluster decay, and alpha decay in the superheavy nuclei of $Z = 122$.

II. THEORETICAL FRAMEWORK

A. Projectile-target combinations to synthesize SHN Z = 122 via fusion

The interacting potential barrier for two spherical nuclei is given by

$$V = V_N(R) + V_C(R) + \frac{\hbar^2 l(l+1)}{2\mu \times r^2}, \tag{1}$$

where l represents the angular momentum and μ is the reduced mass. Coulomb potential $V_c(R)$ is calculated by

$$V_C(R) = Z_1 Z_2 e^2 \begin{cases} \frac{1}{R} & (R > R_C) \\ \frac{1}{2R_c}\left[3 - \left(\frac{R}{R_c}\right)^2\right] & (R < R_C) \end{cases} \tag{2}$$

where $R_C = 1.24 \times (R_1 + R_2)$, R_1 and R_2 are respectively the radii of the emitted alpha and daughter nuclei. Here Z_1 and Z_2 are the atomic numbers of the daughter and emitted cluster.

The nuclear potential is calculated from the proximity potential [29] and it is given as

$$V_p(z) = 4\pi\gamma b\left[\frac{C_1 C_2}{C_1 + C_2}\right]\Phi\left(\frac{z}{b}\right) \tag{3}$$

with the nuclear surface tension coefficient,

$$\gamma = 0.9517[1 - 1.7826(N-Z)^2/A^2]\ \mathrm{MeV/fm^2}. \tag{4}$$

Here N, Z, and A represent the neutron, proton, and mass number of the parent and Φ represents the universal proximity potential [30] and the recent proximity function is

$$\Phi(\varepsilon) = \frac{p_1}{1 + \exp\left(\frac{s_0 + p_2}{p_3}\right)}. \tag{5}$$

Here p_1, p_2, and p_3 are -7.65, 1.02, and 0.89, respectively [31], and s_0 is calculated by the equation

$$s_0 = (R - R_1 - R_2)/b. \tag{6}$$

The width (diffuseness) of the nuclear surface $b \approx 1$ and the Süsmann central radii C_i of the fragments is related to the sharp radii R_i as

$$C_i = R_i - \left(\frac{b^2}{R_i}\right). \tag{7}$$

For R_i, we use a semiempirical formula in terms of mass number A_i as [32]

$$R_i = 1.28A_i^{1/3} - 0.76 + 0.8A_i^{-1/3}. \tag{8}$$

After calculation of the total potential, fusion barriers are estimated. Since fusion happens at a distance larger than the touching configuration of the colliding pair, the above form of the Coulomb potential is justified. One can extract the barrier height V_B and barrier position R_B using the following conditions:

$$\left.\frac{dV(r)}{dr}\right|_{r=R_B} = 0 \quad \text{and} \quad \left.\frac{d^2V(r)}{dr^2}\right|_{r=R_B} \leqslant 0. \tag{9}$$

To study the fusion cross sections, we shall use the model given by Wong [33]. In this formalism, the cross section for complete fusion is given by

$$\sigma_{\text{fus}} = \frac{\pi\hbar^2}{2\mu \times E_{\text{cm}}} \sum_{l=0}^{l_{\max}} (2l+1) \times T_l(E_{\text{cm}}) P_{\text{CN}}(E_{\text{cm}}, l), \tag{10}$$

where μ is the reduced mass. The center of mass energy is denoted by E_{cm}. In the above formula, $l_{\max}$ corresponds to the largest partial wave for which a pocket still exists in the interaction potential and $T_l(E_{\text{cm}})$ is the energy-dependent barrier penetration factor. P_{CN} is the probability for the compound nucleus (CN) formation by two nuclei coming in contact. The probability of compound nucleus formation P_{CN} suggested by previous workers [34–40] is used in the present calculation. The calculation of P_{CN} requires effective fissility which in turn depends on x_{thr} and c. x_{thr} and c are adjustable parameters [22–24]. These parameters were suggested by Loveland [41]. This form of energy dependence of fusion probability is similar to the one proposed by Zargrebeav and Greiner [41].

After the fusion of two nuclei, the corresponding compound nuclei come to the ground state by emitting neutrons. The evaporation residue cross section of SH element production in a heavy-ion fusion reaction with subsequent emission of x neutrons is given by [41]

$$\sigma_{ER}^{xn} = \frac{\pi}{k^2} \sum_{l=0}^{\infty} (2l+1) T(E,l) P_{\text{CN}}(E,l) P_{\text{sur}}^{xn}(E^*, l). \tag{11}$$

P_{sur} is the survival probability and it is the compound nucleus to decay to the ground state of the final residual nucleus via evaporation of neutrons/light particles. The survival probability is the probability that the fused system emits several neutrons followed by observing a sequence of α decay from the residue. The survival probability under the evaporation of x neutrons is

$$P_{\text{sur}} = P_{\text{xn}}(E_{\text{CN}}^*) \prod_{i=1}^{i_{\max}=x} \left(\frac{\Gamma_n}{\Gamma_n + \Gamma_f}\right)_{i,E^*}, \tag{12}$$

where the index "i" is equal to the number of emitted neutrons. The calculation of P_{sur} requires the probability of evaporation of x neutrons from the compound nucleus (P_{xn}). To calculate the P_{xn}, we have adopted the procedure explained by previous workers [39,40]. The term $[\Gamma_n/(\Gamma_n + \Gamma_f)]$ in Eq. (12) is calculated by the knowledge of the ratio of the emission width of a neutron to the fission width (Γ_n/Γ_f). In the present work, we have used the expression for Γ_n/Γ_f based on the level densities of the Fermi-gas model [40].

B. Competition between binary fission, ternary fission, cluster radioactivity, and alpha decay process in superheavy nuclei

The interacting potential between two nuclei of fission fragments is taken as the sum of the Coulomb potential and proximity potential. To study the ternary and binary fission, we have used Denisov nuclear potential $Vp(r)$ [42] and it is given by

$$\begin{aligned} V_P(r) = {} & -1.989\,843 \frac{R_1 R_2}{R_1 + R_2} \varphi(r - R_1 - R_2 - 2.65) \\ & \times \left[1 + 0.003\,525\,139 \left(\frac{A_1}{A_2} + \frac{A_2}{A_1}\right)^{3/2} \right. \\ & \left. - 0.411\,326\,3(I_1 + I_2)\right], \end{aligned} \tag{13}$$

where the effective nuclear radius is given by

$$\begin{aligned} R_i = {} & R_{ip}\left(1 - \frac{11.654\,15}{R_{ip}}\right) \\ & + 1.284\,589\left(I_i - \frac{0.4A_i}{A_i + 200}\right) (i = 1, 2), \end{aligned} \tag{14}$$

where R_{ip} is given by

$$\begin{aligned} R_{ip} &= 1.24A_i^{3/2}\left[1 + \frac{1.646}{A_i} - 0.191\left(\frac{A_i - 2Z_i}{A_i}\right)\right] \quad \text{with} \\ I_i &= \frac{N_i - Z_i}{A_i}. \end{aligned} \tag{15}$$

The universal function $\phi(s = r - R_1 - R_2 - 2.65)$ is given by

$$\Phi(\xi) = \begin{cases} 1 - s/0.788\,166\,3 + 1.229\,218S^2 - 0.223\,427\,7S^3 - 0.103\,876\,9S^4 \\ -\frac{R_1R_2}{R_1+R_2}(0.184\,493\,5S^2 + 0.075\,701\,01S^3) + (I_1 + I_2)(0.044\,706\,45S^2 + 0.033\,468\,70S^3) & \text{for } -5.65 \leqslant S \leqslant 0 \\ 1 - S^2\left[0.054\,101\,06\frac{R_1R_2}{R_1+R_2}\exp\left(-\frac{S}{1.760\,580}\right)\right] \\ -0.539\,542\,0(I_1 + I_2)\exp\left(-\frac{S}{2.424\,408}\right) \times \exp\left(-\frac{S}{0.788\,166\,3}\right) & \text{for } S \geqslant 0 \end{cases}.$$

To study the cluster decay and alpha decay, Coulomb potential $V_c(R)$ is taken as

$$V_C(R) = Z_1 Z_2 e^2 \begin{cases} \frac{1}{R} & (R > R_C) \\ \frac{1}{2R_c}\left[3 - \left(\frac{R}{R_c}\right)^2\right] & (R < R_C) \end{cases}, \tag{16}$$

where $R_C = 1.24 \times (R_1 + R_2)$, R_1 and R_2 are respectively the radii of the emitted alpha/cluster and daughter nuclei. Here Z_1 and Z_2 are the atomic numbers of the daughter and emitted cluster. We have used the proximity function defined specially for cluster/alpha decay and it is given as [30]

$$\Phi(\varepsilon) = \frac{p_1}{1 + \exp\left(\frac{s_0 + p_2}{p_3}\right)} \quad \text{with} \quad s_0 = \frac{R - R_1 - R_2}{b}. \tag{17}$$

Here p_1, p_2, and p_3 are −7.65, 1.02, and 0.89, respectively [31].

For all four processes such as spontaneous fission, alpha ternary fission, cluster decay, and alpha decay, the barrier penetrability P is given as

$$P = \exp\left\{-\frac{2}{\hbar}\int_a^b \sqrt{2\mu(V - Q)}dz\right\}. \tag{18}$$

Here $\mu = mA_1A_2/A$, where m is the nucleon mass and A_1, A_2 are the mass numbers of daughter and emitted clusters, respectively. For cluster/alpha decay, the turning points "a" and "b" are determined from the equation, $V(a) = V(b) = Q$. For the fission process, the first turning point is determined from the equation $V(a) = Q$ and the second turning point from $b = 0$. The above integral can be evaluated numerically or analytically, and the half-life time is given by

$$T_{1/2} = \frac{\ln 2}{\lambda} = \frac{\ln 2}{\upsilon P}, \tag{19}$$

where $\upsilon = \frac{\omega}{2\pi} = \frac{2E_\upsilon}{h}$ represents the number of assaults on the barrier per second and λ is the decay constant. E_υ, the empirical vibration energy, is given as

$$E_\upsilon = Q\left\{0.056 + 0.039\exp\left[\frac{4 - A_2}{2.5}\right]\right\} \quad \text{for} \quad A_2 \geqslant 4. \tag{20}$$

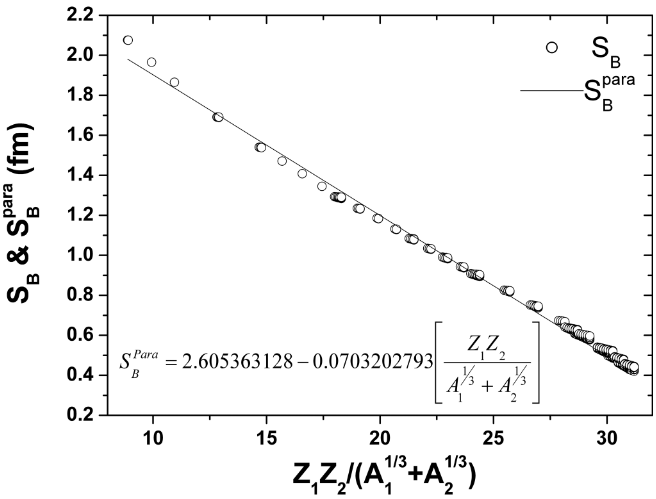

FIG. 3. Reduced fusion barrier positions S_B(fm) as a function of $\frac{Z_1 Z_2}{A_1^{1/3}+A_2^{1/3}}$.

III. RESULTS AND DISCUSSION

In the previous study [26], it is observed that the nuclei $^{307-314}122$ were found to have long half-lives and hence it could be sufficient to detect them if synthesized in a laboratory. To check isotopes for the stability against the proton, neutron, and beta emission, we have calculated the corresponding separation energies. The calculated separation energies for different isotopes of superheavy nuclei $Z = 122$ are shown in Fig. 2. On calculating the separation energies for the isotopes of $Z = 122$, the two-proton separation energy $S(2p)$ is negative

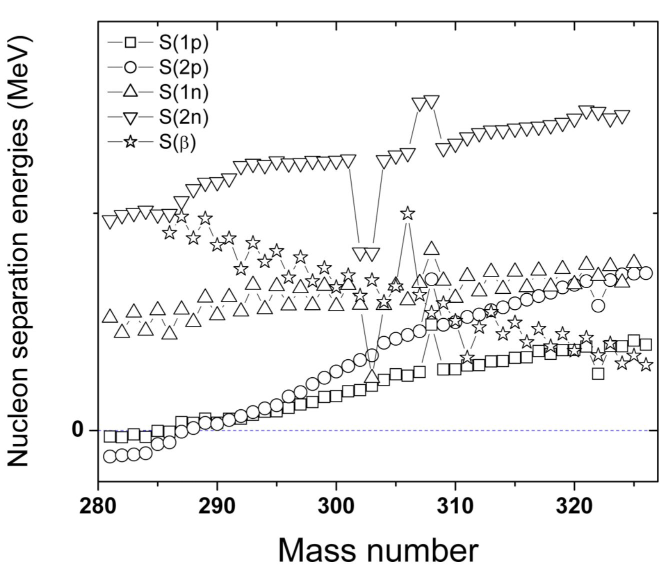

FIG. 2. Nucleon separation energies as a function of mass number for $Z = 122$.

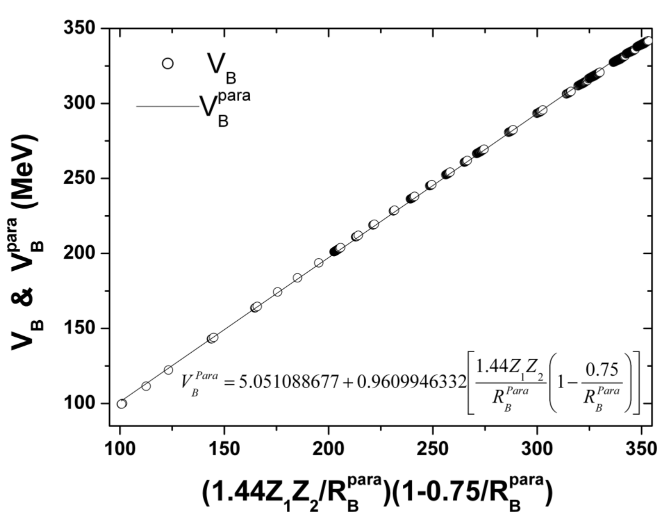

FIG. 4. Fusion barrier heights V_B(MeV) as a function of $\frac{Z_1 Z_2}{R_B^{\rm par}}(1 - \frac{1}{R_B^{\rm par}})$.

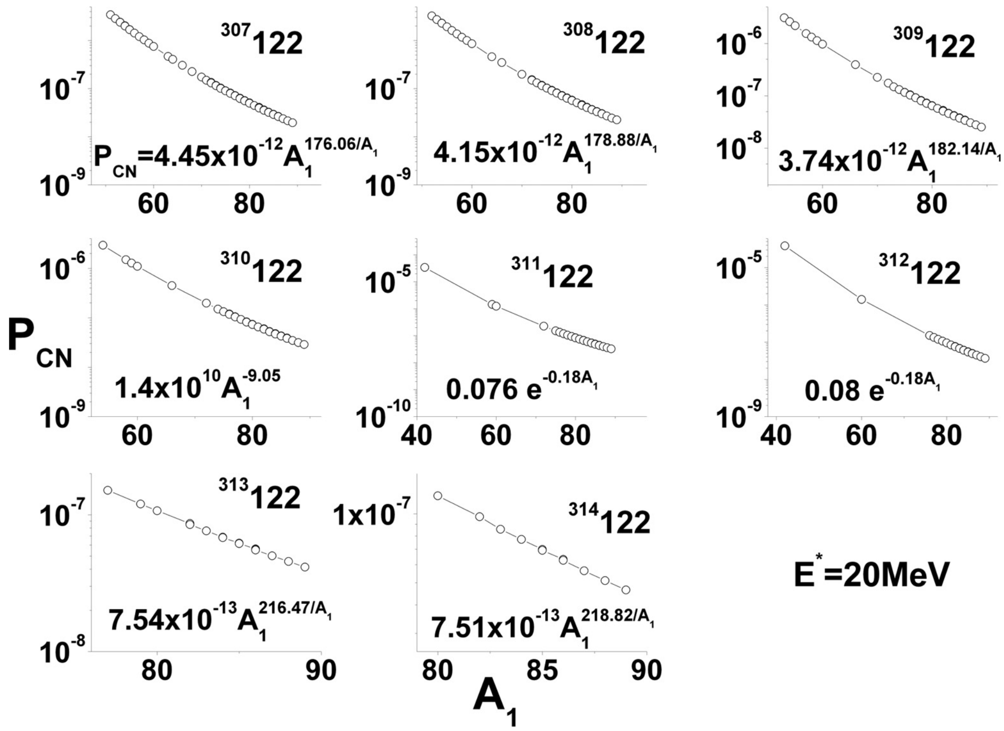

FIG. 5. Variation of compound nucleus probability (P_{CN}) at 20 MeV with mass number of projectile.

for those isotopes within the range $280 \leqslant A \leqslant 289$. These observations make it clear that all those isotopes within the range $280 \leqslant A \leqslant 289$ are outside the proton drip line and thus may easily decay through proton emission. Hence the nuclei $^{307\text{–}314}$122 may not undergo proton, neutron, and beta decay.

After identifying the most probable isotopes for the superheavy element $Z = 122$, we have studied the possible fusion reactions for their synthesis. We have studied around 900 possible projectile target combinations to synthesize superheavy nuclei $^{307\text{–}314}$122. For all projectile-target combinations, we have

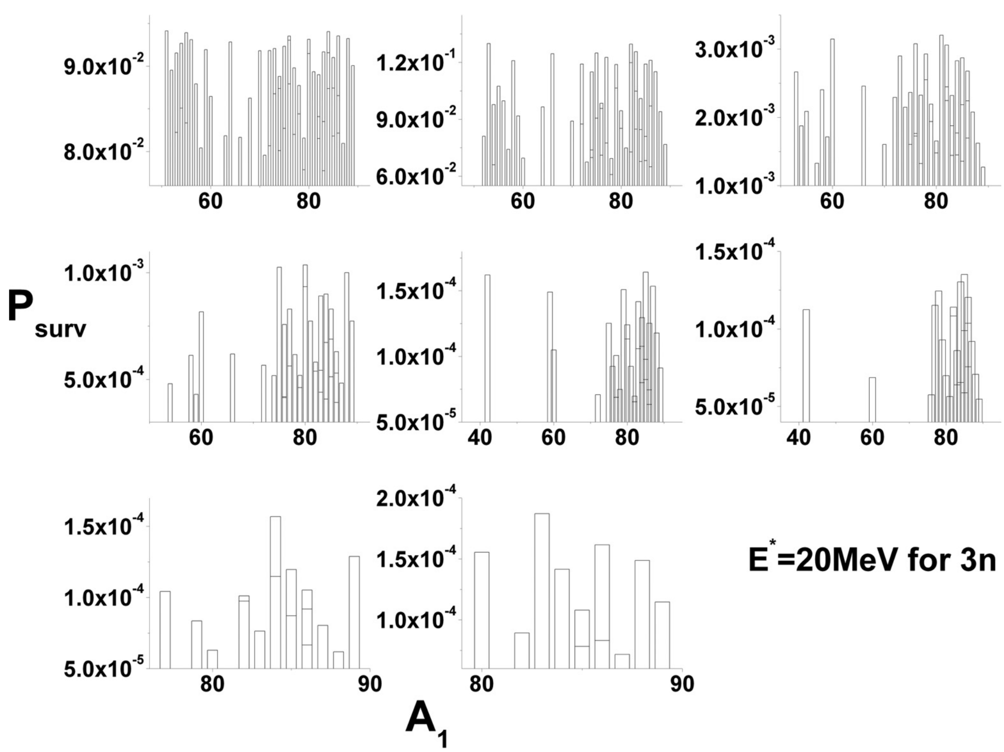

FIG. 6. Variation of survival probability (P_{Surv}) at 20 MeV (for $3n$ evaporation channel) with mass number of projectile.

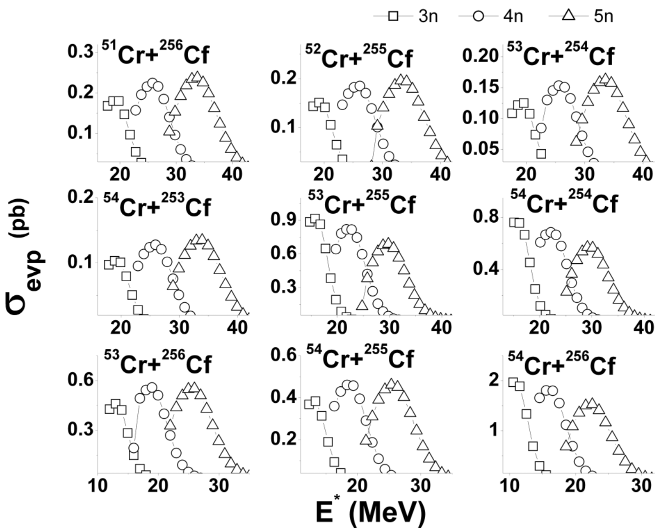

FIG. 7. Evaporation residue cross section as a function of E^* for projectile-target combination Cr + Cf.

calculated the fusion barrier heights (V_B) and positions (R_B). Once fusion barrier heights and positions were calculated, a search was made for their parametrization. We have calculated the reduced fusion barrier $S_B = R_B - C_1 - C_2$ and plotted reduced fusion barrier as a function of $Z_1Z_2/(A_1^{1/3} + A_2^{1/3})$ and it is shown in Fig. 3. We have fitted the function for the reduced fusion barrier in terms of $Z_1Z_2/(A_1^{1/3} + A_2^{1/3})$ as follows:

$$S_B^{\text{para}} = 2.6054 - 0.0703 \times \left[\frac{Z_1Z_2}{A_1^{1/3} + A_2^{1/3}}\right], \tag{21}$$

hence the fusion barrier position (R_B) becomes $R_B^{\text{para}} = S_B^{\text{para}} + C_1 + C_2$.

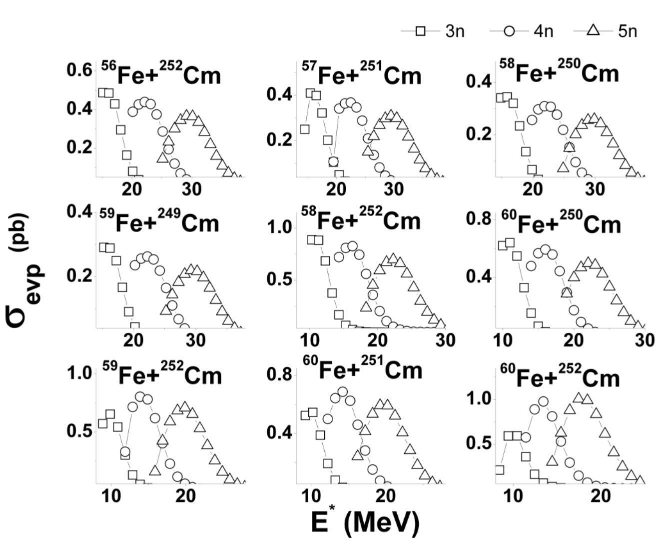

FIG. 8. Evaporation residue cross section as a function of E^* for projectile-target combination Fe + Cm.

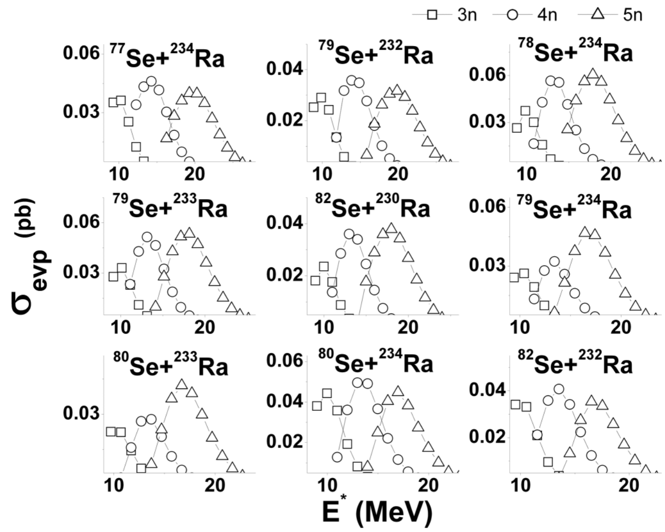

FIG. 9. Evaporation residue cross section as a function of E^* for projectile-target combination Se + Ra.

Finally, the parametrized fusion barrier position can be expressed as

$$R_B^{\text{para}} = 2.6054 - 0.0703 \times \left[\frac{Z_1Z_2}{A_1^{1/3} + A_2^{1/3}}\right] + C_1 + C_2. \tag{22}$$

The calculated fusion barrier height (V_B) is plotted as a function of $(Z_1Z_2/R_B^{\text{para}})(1 - 1/R_B^{\text{para}})$ and it is shown in Fig. 4. We have fitted nonlinear function for fusion barrier height as follows;

$$V_B^{\text{para}} = 5.051 + 0.961\left[\frac{1.44Z_1Z_2}{R_B^{\text{para}}}\left(1 - \frac{0.75}{R_B^{\text{para}}}\right)\right]. \tag{23}$$

The above equations may be used to produce the barrier heights (V_B) and the positions (R_B) of $^{307-314}122$ nuclei. After

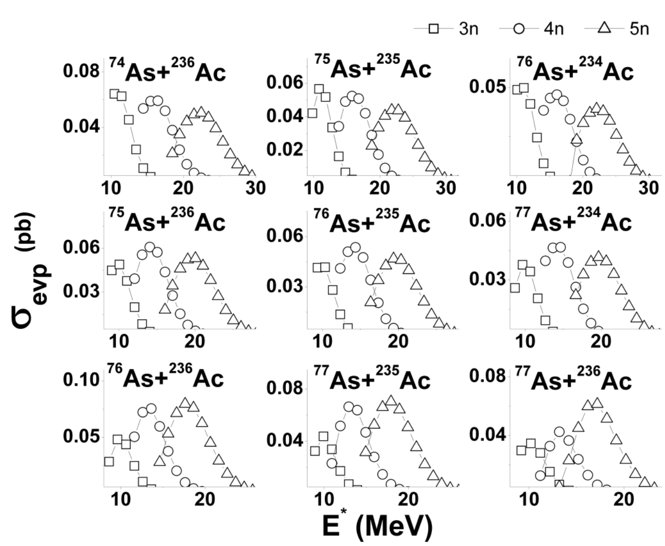

FIG. 10. Evaporation residue cross section as a function of E^* for projectile-target combination As + Ac.

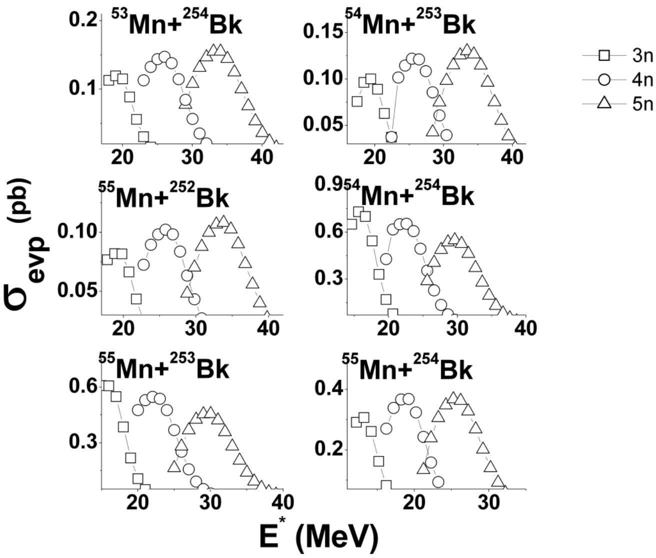

FIG. 11. Evaporation residue cross section as a function of E^* for projectile-target combination Mn + Bk.

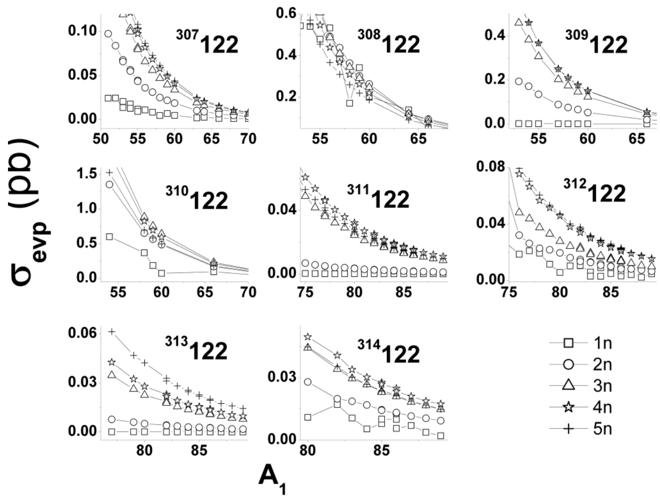

FIG. 12. Evaporation residue cross section as a function of mass number of the projectile.

studying the fusion barriers, we have calculated the compound nucleus formation probability (P_{CN}) and the survival probability for different projectile-target combinations.

The variation of calculated compound nucleus formation probability (P_{CN}) at 20 MeV with a mass number of projectile for superheavy nuclei $^{307-314}122$ is shown in Fig. 5. From this figure, it is clear that P_{CN} decreases with increasing mass number of projectile. The variation of survival probability (P_{Surv}) at 20 MeV (for $3n$) with mass number of projectile for superheavy nuclei $^{307-314}122$ is as shown in Fig. 6. We have calculated the evaporation residue cross sections for all studied possible projectile target combinations to synthesize superheavy nuclei $^{307-314}122$. Figures 7–11 show the evaporation residue cross section as a function of E^* for projectile-target combination systems Cr + Cf, Fe + Cm, Se + Ra, As + Ac, and Mn + Bk respectively.

We have studied the variation of evaporation residue cross section as a function of mass number. Figure 12 shows the variation of evaporation residue cross section for $^{307-314}122$ vs mass number of the projectiles. The evaporation residue cross section decreases with increase in the mass number of the projectiles. We have selected the most probable projectile-target combination to synthesize superheavy nuclei $^{307-314}122$ that have minimum driving potential, maximum fusion, and evaporation residue cross sections. The selected most probable projectile-target combinations such as Cr + Cf, Fe + Cm, Se + Ra, As + Ac are listed in Table I.

The parameters required to decide the synthesis of superheavy nuclei such as compound nucleus fissility (χ_{CN}), charge product in the entrance channel (Z_pZ_t), effective entrance channel fissility (χ_{eff}), fusion barrier height (V_B), and fusion barrier width (R_B) for the most probable fusion reactions are also shown in Table I. The compound nucleus fissility (χ_{CN}) is calculated using the following equation:

$$\chi_{\mathrm{CN}} = \frac{Z^2}{A} \Big/ \left(\frac{Z^2}{A}\right)_{\mathrm{crit}}, \tag{24}$$

where Z and A are the atomic and mass numbers of the compound nucleus, respectively. The denominator is taken as

$$\left(\frac{Z^2}{A}\right)_{\mathrm{crit}} = 50.883(1 - 1.7826 I^2), \tag{25}$$

where $I = (A - 2Z)/A$ is the relative neutron excess of the compound nucleus.

The effective entrance channel fissility (χ_{eff}) is defined as

$$\chi_{\mathrm{eff}} = \frac{4Z_1Z_2}{\left[A_1^{1/3}A_2^{1/3}\left(A_1^{1/3} + A_2^{1/3}\right)\right]} \Big/ \left(\frac{Z^2}{A}\right)_{\mathrm{crit}}, \tag{26}$$

where A_1 and A_2 are the mass number of projectile and target nucleus respectively. Tabulated data of compound nucleus fissility (χ_{CN}), charge product in the entrance channel (Z_pZ_t), effective entrance channel fissility (χ_{eff}), fusion barrier height (V_B), and fusion barrier width (R_B) for the most probable fusion reactions are useful in the experiments to synthesize more isotopes of SHN $Z = 122$.

After identifying the most probable projectile-target combinations, we have studied the different decay modes of $Z = 122$. The formed compound nucleus may undergo different decay modes such as alpha decay, cluster decay, and binary and ternary fission processes. It is essential to study the competition between different decay modes of superheavy nuclei. The energy released (Q) during the studied process such as spontaneous fission, alpha ternary fission, cluster decay, and alpha decay is calculated by using the following equation:

$$Q = \Delta M(A, Z) - \sum_{i}^{n} \Delta M(A_i, Z_i), \tag{27}$$

where $\Delta M(A, Z)$ and $\Delta M(A_i, Z_i)$ are the mass excess of the parent and emitted nuclei respectively.

For ternary fission n varies from 1 to 3. For spontaneous fission and cluster and alpha decay processes, n varies from 1 to 2. In the present work, we have used this experimental mass excess data [43]. Some of the experimental mass excess values are not available. For those nuclei, where experimental

TABLE I. Presynthesis parameters for SHE $Z = 122$.

CN	Most probable projectile-target combination	$(\sigma_{\mathrm{Evp}})_{\max}$ pb	V_B (MeV)	R_B (fm)	$Z_p Z_t$	χ_{CN}	χ_{eff} ($\times 10^3$)	$E_{c.m}$ (MeV)	N/A
	^{57}Fe (S 2.12%) + ^{250}Cm(9000 yr)	5.61×10^{-2}	268.731	12.338	2496		1.31	288	
	^{60}Fe (2.6×10^6 yr) + ^{247}Cm (1.56×10^7 yr)	3.38×10^{-2}	267.65	12.397	2496		1.26	287	
^{307}122	^{63}Ni (100 yr) + ^{244}Pu (8.08×10^7 yr)	1.92×10^{-2}	282.425	12.361	2632	1.0302	1.28	302	0.6026
	^{72}Zn (S 46.5%) + ^{235}U (7.04×10^8 yr)	4.80×10^{-3}	294.373	12.423	2760		1.22	314	
	^{79}Se (3.27×10^5 yr) + ^{228}Ra (5.75 yr)	1.80×10^{-3}	319.253	12.357	2992		1.24	339	
	^{58}Fe (S 0.28%) + ^{250}Cm (9000 yr)	3.45×10^{-1}	268.141	12.37	2496		1.29	284	
	^{60}Fe (2.6×10^6 yr) + ^{248}Cm (3.4×10^5 yr)	2.47×10^{-1}	267.429	12.409	2496		1.25	283	
	^{64}Ni (S 0.926%) + ^{244}Pu (8.08×10^7 yr)	1.21×10^{-1}	281.845	12.391	2632		1.26	297	
^{308}122	^{70}Zn (S 0.65%) + ^{238}U (4.468×10^9 yr)	4.67×10^{-2}	294.741	12.405	2760	1.0289	1.24	310	0.6039
	^{72}Zn (S 46.5%) + ^{236}U (2.342×10^7 yr)	3.55×10^{-2}	294.121	12.436	2760		1.21	310	
	^{76}Ge (1.78×10^{21} yr) + ^{232}Th (1.41×10^{10} yr)	1.98×10^{-2}	306.834	12.412	2880		1.22	322	
	^{80}Se (S 49.85%) + ^{228}Ra (5.75 yr)	1.15×10^{-2}	318.685	12.385	2992		1.23	334	
	^{82}Se (1.08×10^{20} yr) + ^{226}Ra (1600 yr)	9.10×10^{-3}	318.129	12.412	2992		1.21	334	
	^{53}Cr (S 9.5%) + ^{256}Cf (12.3 min)	4.60×10^{-1}	253.032	12.374	2352		1.29	266	
	^{54}Cr (S 2.365%) + ^{255}Cf (85 min)	3.83×10^{-1}	252.656	12.395	2352		1.27	266	
	^{57}Fe (S 2.12%) + ^{252}Cm (<1 d)	2.03×10^{-1}	268.289	12.362	2496		1.30	281	
	^{58}Fe (S 0.28%) + ^{251}Cm (16.2 min)	1.74×10^{-1}	267.921	12.382	2496		1.28	281	
	^{59}Fe (44.6 d) + ^{250}Cm (9000 yr)	1.46×10^{-1}	267.561	12.402	2496		1.26	281	
	^{60}Fe (2.6×10^6 yr) + ^{249}Cm (64.15 min)	1.23×10^{-1}	267.209	12.421	2496	1.0277	1.25	280	0.6052
^{309}122	^{66}Ni (54.6 h) + ^{243}Pu (4.956 h)	4.50×10^{-2}	280.945	12.438	2632		1.22	294	
	^{70}Zn (S 0.6%) + ^{239}U (23.45 min)	2.33×10^{-2}	294.49	12.418	2760		1.23	308	
	^{72}Zn (S 46.5%) + ^{237}U (6.75 d)	1.79×10^{-2}	293.871	12.449	2760		1.21	307	
	^{76}Ge (1.78×10^{21} yr) + ^{233}Th (21.83 min)	9.90×10^{-3}	306.568	12.425	2880		1.21	320	
	^{79}Se (3.27×10^5 yr) + ^{230}Ra (92 min)	6.50×10^{-3}	318.692	12.384	2992		1.23	332	
	^{82}Se (1.08×10^{20} yr) + ^{227}Ra (42.2 min)	4.60×10^{-3}	317.849	12.426	2992		1.20	331	
	^{54}Cr (S 2.365%) + ^{256}Cf (12.3 min)	1.97×10^{0}	252.452	12.407	2352		1.27	263	
	^{58}Fe (S 0.28%) + ^{252}Cm (<1 d)	8.88×10^{-1}	267.701	12.395	2496		1.27	278	
	^{59}Fe (44.6 d) + ^{251}Cm (16.8 min)	7.56×10^{-1}	267.341	12.413	2496		1.26	278	
	^{60}Fe (2.6×10^6 yr) + ^{250}Cm (9000 yr)	6.40×10^{-1}	266.99	12.432	2496		1.24	278	
^{310}122	^{66}Ni (54.6 h) + ^{244}Pu (8×10^7 yr)	2.30×10^{-1}	280.711	12.45	2632		1.22	291	
	^{72}Zn (S 46.5%) + ^{238}U (4.468×10^9 yr)	9.19×10^{-2}	293.621	12.462	2760	1.0265	1.20	304	0.6065
	^{76}Ge (1.78×10^{21} yr) + ^{234}Th (24.1 d)	5.15×10^{-2}	306.304	12.438	2880		1.21	317	
	^{75}As (S100%) + ^{235}Ac (40 s)	5.67×10^{-2}	313.219	12.381	2937		1.24	324	
	^{80}Se (S 49.8%) + ^{230}Ra (92 min)	2.99×10^{-2}	318.126	12.412	2992		1.21	329	
	^{82}Se (1.08×10^{20} yr) + ^{228}Ra (5.75 yr)	2.36×10^{-2}	317.569	12.439	2992		1.19	328	
	^{59}Fe (44.6 d) + ^{252}Cm (<1 d)	6.53×10^{-1}	267.123	12.425	2496		1.25	277	
	^{60}Fe (2.6×10^6 yr) + ^{251}Cm (16.8 min)	5.45×10^{-1}	266.771	12.444	2496		1.23	277	
	^{72}Zn (S 46.5%) + ^{239}U (23.45 min)	7.90×10^{-2}	293.373	12.474	2760		1.19	303	
	^{75}As (S 100%) + ^{236}Ac (2 min)	4.89×10^{-2}	312.949	12.394	2937		1.24	323	
	^{76}As (1.1 d) + ^{235}Ac (40 s)	4.18×10^{-2}	312.644	12.409	2937		1.22	323	
^{311}122	^{77}As (38.33 h) + ^{234}Ac (44 s)	3.78×10^{-2}	312.345	12.424	2937	1.0254	1.21	322	0.6077
	^{77}Se (S 7.6%) + ^{234}Ra (30 s)	3.63×10^{-2}	318.729	12.383	2992		1.24	329	
	^{78}Se (S 23.69%) + ^{233}Ra (30 s)	3.22×10^{-2}	318.429	12.397	2992		1.23	328	
	^{79}Se (3.27×10^5 yr) + ^{232}Ra (250 s)	2.91×10^{-2}	318.136	12.412	2992		1.22	328	
	^{80}Se (S 49.8%) + ^{231}Ra (103 s)	2.56×10^{-2}	317.848	12.426	2992		1.21	328	
	^{82}Se (1.08×10^{20} yr) + ^{229}Ra (4 min)	2.04×10^{-2}	317.292	12.453	2992		1.19	327	
	^{60}Fe (2.6×10^6 yr) + ^{252}Cm (<1 d)	5.91×10^{-1}	266.554	12.456	2497		1.23	277	
	^{76}As (1.1 d) + ^{236}Ac (2 min)	4.81×10^{-2}	312.375	12.423	2937		1.22	322	
	^{77}As (38.33 h) + ^{235}Ac (40 s)	4.38×10^{-2}	312.076	12.437	2937		1.21	322	
^{312}122	^{78}Se (S 23.69%) + ^{234}Ra (30 s)	3.75×10^{-2}	318.154	12.411	2992	1.0243	1.22	328	0.6090
	^{79}Se (3.27×10^5 yr) + ^{233}Ra (30 s)	3.30×10^{-2}	317.86	12.425	2992		1.21	328	
	^{80}Se (S 49.8%) + ^{232}Ra (250 s)	2.78×10^{-2}	317.572	12.439	2992		1.20	328	
	^{82}Se (1.08×10^{20} yr) + ^{230}Ra (92 min)	2.36×10^{-2}	317.015	12.466	2992		1.18	327	

TABLE I. (*Continued.*)

CN	Most probable projectile-target combination	$(\sigma_{\mathrm{Evp}})_{\max}$ Pb	V_B (MeV)	R_B (fm)	Z_pZ_t	χ_{CN}	χ_{eff} $(\times 10^3)$	$E_{c.m}$ (MeV)	N/A
^{313}122	^{77}As (38.33 h) + ^{236}Ac (2 min)	3.46×10^{-2}	311.809	12.451	2937	1.0232	1.20	322	0.6102
	^{79}Se (3.27×10^5 yr) + ^{234}Ra (30 s)	2.62×10^{-2}	317.585	12.438	2992		1.20	328	
	^{80}Se (S 49.8%) + ^{233}Ra (30 s)	2.25×10^{-2}	317.298	12.453	2992		1.19	327	
	^{82}Se (1.08×10^{20} yr) + ^{231}Ra (103 s)	1.86×10^{-2}	316.74	12.48	2992		1.17	327	
^{314}122	^{80}Se (S 49.8%) + ^{234}Ra (30 s)	4.44×10^{-2}	317.024	12.466	2992	1.0221	1.19	327	0.6115
	^{82}Se (1.08×10^{20} yr) + ^{232}Ra (250 s)	3.41×10^{-2}	316.467	12.493	2992		1.17	326	

mass excess was unavailable, we have used theoretical values [44,45]. The total potential for spontaneous and ternary fission of different fission fragments are calculated. The driving potential $(V-Q)$ is calculated. The variation of driving potential for spontaneous and ternary fission as a function of the mass number of fragment A_1 is shown in Fig. 13. The calculated spontaneous and ternary fission half-lives for the combination of different fission fragments of superheavy nuclei $Z=122$ are presented. The variation of logarithmic half-lives of spontaneous and ternary fission as a function of mass number A_1 for different isotopes of SHN $Z=122$ are shown in Fig. 14.

The energy released (Q) during the emission of different cluster nuclei from the different isotopes of SHN $Z=126$ is calculated. Figure 15 represents the energy released (Q) during the emission of different clusters ($^{12\text{–}14}$C, ^{14}N, $^{20\text{–}24}$Ne, $^{28\text{–}34}$Si, $^{36\text{–}44}$Ar, $^{40\text{–}48}$Ca) from the superheavy nuclei $Z=122$ as a function of mass number of clusters. From this figure, it is clear that the Q value in the cluster decay increases with an increase in the mass number of the emitted cluster. The half-lives of cluster emission ($^{12\text{–}14}$C, ^{14}N, $^{20\text{–}24}$Ne, $^{28\text{–}34}$Si, $^{36\text{–}44}$Ar, $^{40\text{–}48}$Ca) from the different isotopes of superheavy nuclei $Z=122$ are calculated. Figure 16 shows the variation of logarithmic half-lives for the emission of different clusters ($^{12\text{–}14}$C, ^{14}N, $^{20\text{–}24}$Ne, $^{28\text{–}34}$Si, $^{36\text{–}44}$Ar, $^{40\text{–}48}$Ca) from superheavy nuclei $Z=122$ as a function of mass number of daughter nuclei.

The computed logarithmic cluster decay half-lives, decay constant, barrier penetrability, and other characteristics of cluster decay during the emission of ^{12,14}C, ^{14}N, ^{20,22,24}Ne, ^{28,30,32,34}Si, ^{36,38,40,42,44}Ar, ^{40,42,44,46,48}Ca from the different isotopes of superheavy nuclei $Z=122$ are tabulated in the Table II. To identify the dominant decay mode of the most predicted isotopes of superheavy nuclei $Z=122$, we have calculated the branching ratios. Branching ratios are calculated using their decay constants. The branching ratio of alpha decay with respect to spontaneous fission is defined as

$$\mathrm{BR}=\frac{\lambda_\alpha}{\lambda_{\mathrm{SF}}}. \tag{28}$$

The branching ratio of alpha decay with respect to alpha ternary fission is defined as

$$\mathrm{BR}=\frac{\lambda_\alpha}{\lambda_{\mathrm{TF}}}. \tag{29}$$

The branching ratio of alpha decay with respect to cluster decay is defined as

$$\mathrm{BR}=\frac{\lambda_\alpha}{\lambda_{\mathrm{CR}}}, \tag{30}$$

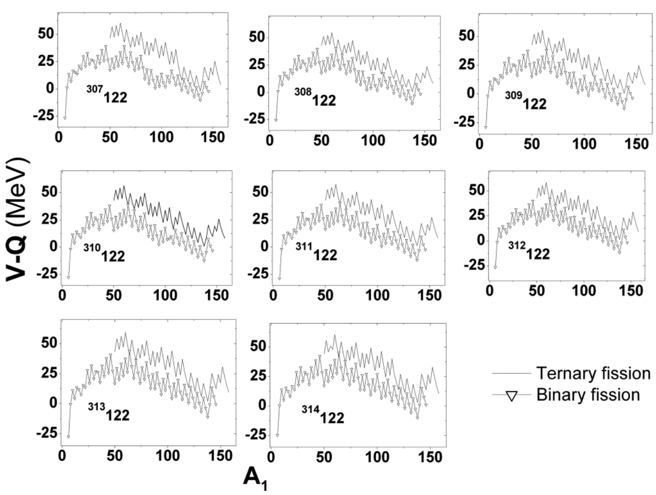

FIG. 13. Variation of driving potential for spontaneous and ternary fission as a function of the mass number of fragment A_1.

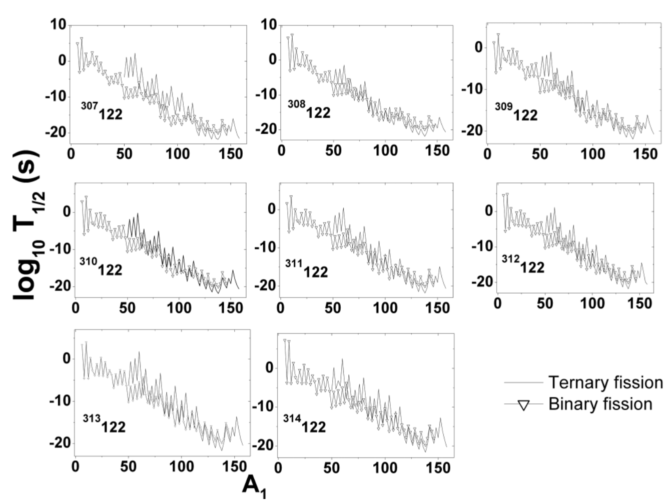

FIG. 14. Variation of logarithmic half-lives of spontaneous and ternary fission as a function of mass number A_1 for different isotopes of SHN $Z=122$.

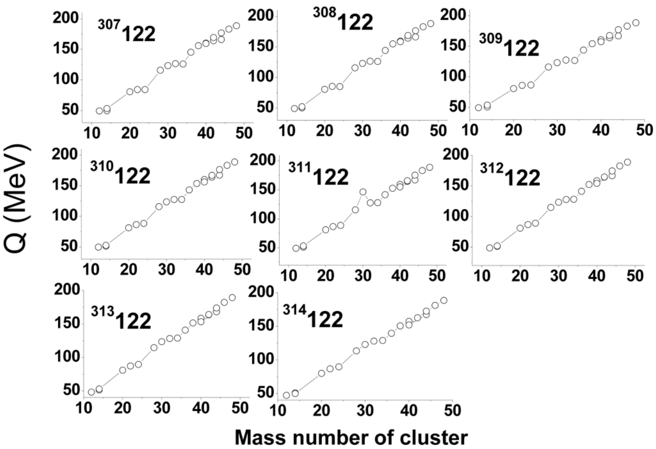

FIG. 15. Energy released (Q) during the emission of different clusters ($^{12-14}C$, ^{14}N, $^{20-24}Ne$, $^{28-34}Si$, $^{36-44}Ar$, $^{40-48}Ca$) for superheavy nuclei $Z = 122$ as a function of mass number of clusters.

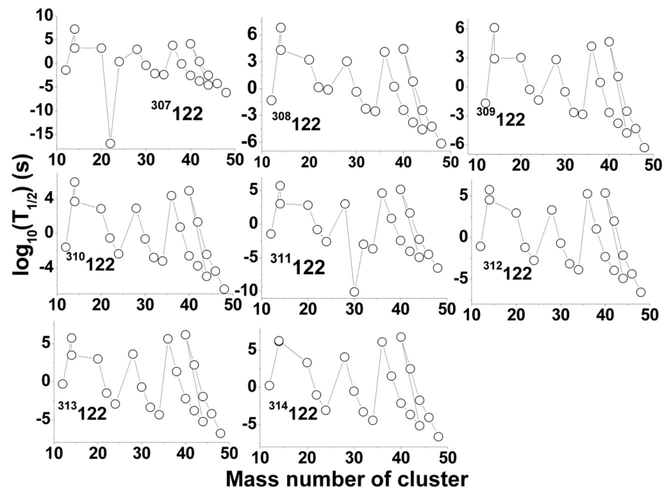

FIG. 16. Variation of logarithmic half-lives for the emission of different clusters ($^{12-14}C$, ^{14}N, $^{20-24}Ne$, $^{28-34}Si$, $^{36-44}Ar$, $^{40-48}Ca$) from superheavy nuclei $Z = 122$ as a function of mass number of cluster nuclei.

where λ_α, λ_{SF}, λ_{TF}, and λ_{CR} are decay constants, corresponds to alpha decay, spontaneous fission, alpha ternary fission, and cluster decay processes respectively. The calculated branching ratio of alpha decay with respect to the spontaneous fission, ternary fission, and cluster decay for different isotopes of superheavy nuclei $Z = 122$ is as shown in Table III. The computed logarithmic half-life values for various decay modes of superheavy nuclei $Z = 122$ is as given in Table IV. We have compared the logarithmic half-lives for spontaneous fission, ternary fission, cluster radioactivity, and alpha decay for superheavy nuclei $^{307}126$, $^{318}126$, $^{319}126$, $^{320}126$, and $^{323-326}126$ and it is shown in Table IV. From this table, it is clear that alpha decay half-lives are smaller than those of spontaneous fission, ternary fission, and cluster decay for the isotopes of superheavy nuclei $Z = 122$.

IV. CONCLUSION

We have also selected the most probable projectile-target combinations, Cr + Cf, Fe + Cm, Se + Ra, As + Ac to synthesize the superheavy element $Z = 122$. We hope that our predictions may be a guide for future experiments in the synthesis of more isotopes of superheavy nuclei $Z = 112$. We have also studied the different decay modes of the most predicted isotopes of superheavy element $Z = 122$. The comparison of half-lives for different decay modes reveals that alpha decay has smaller half-lives than the other studied decay modes. A detailed study of branching ratio of alpha decay with respect to other decay modes also confirms that alpha decay is the most dominant decay mode for the isotopes of superheavy nuclei $^{307-314}122$ and hence these nuclei can be detected through the alpha decay mode only.

TABLE II. The computed logarithmic half-life values, decay constant, barrier penetrability and other characteristics, and cluster decay during the emission of $^{12,14}C$, ^{14}N, $^{20,22,24}Ne$, $^{28,30,32,34}Si$, $^{36,38,40,42,44}Ar$, $^{40,42,44,46,48}Ca$ from the different isotopes of superheavy nuclei $Z = 122$.

Parent nuclei	Emitted cluster	Daughter nuclei	Q value(MeV)	Penetrability P	Decay constant λ	$\log_{10} T_{1/2}$	Parent nuclei
	^{12}C	$^{295}122$	49.3300	1.34×10^{21}	1.15×10^{-20}	1.54×10^{1}	−1.347
	^{14}C	$^{293}122$	49.5100	1.34×10^{21}	2.54×10^{-29}	3.41×10^{-8}	7.307929
	^{14}N	$^{293}122$	53.2070	1.44×10^{21}	2.44×10^{-25}	3.51×10^{-4}	3.294449
	^{20}Ne	$^{287}122$	80.5120	2.18×10^{21}	1.76×10^{-25}	3.83×10^{-4}	3.256649
	^{22}Ne	$^{285}122$	84.1380	2.28×10^{21}	2.22×10^{-5}	2.81×10^{-4}	−16.8631
	^{24}Ne	$^{283}122$	84.2190	2.28×10^{21}	1.13×10^{-22}	6.78×10^{-21}	0.428553
	^{28}Si	$^{279}122$	115.8330	3.14×10^{21}	2.07×10^{-25}	6.50×10^{-4}	3.027158
	^{30}Si	$^{277}122$	123.1470	3.33×10^{21}	4.83×10^{-22}	0.161×10^{1}	−0.36646
$^{307}122$	^{32}Si	$^{275}122$	126.4180	3.42×10^{21}	2.52×10^{-20}	8.63×10^{1}	−2.09612
	^{34}Si	$^{273}122$	125.9880	3.41×10^{21}	4.24×10^{-20}	3.41×10^{21}	−2.32031
	^{36}Ar	$^{271}122$	145.1920	3.93×10^{21}	2.55×10^{-26}	1.00×10^{-4}	3.839018
	^{38}Ar	$^{269}122$	155.7450	4.22×10^{21}	1.86×10^{-22}	7.84×10^{-1}	−0.05432
	^{40}Ar	$^{267}122$	160.1260	4.34×10^{21}	4.83×10^{-20}	2.09×10^{2}	−2.48052
	^{42}Ar	$^{265}122$	164.0040	4.44×10^{21}	7.63×10^{-19}	3.39×10^{3}	−3.68996
	^{44}Ar	$^{263}122$	166.1260	4.5×10^{21}	5.07×10^{-18}	2.28×10^{4}	−4.51753

TABLE II. (*Continued.*)

Parent nuclei	Emitted cluster	Daughter nuclei	Q value(MeV)	Penetrability P	Decay constant λ	$\log_{10} T_{1/2}$	Parent nuclei
	^{40}Ca	^{267}122	159.3960	4.32×10^{21}	1.07×10^{-26}	4.61×10^{-5}	4.176363
	^{42}Ca	^{265}122	169.3870	4.59×10^{21}	4.95×10^{-23}	2.27×10^{-1}	0.483641
	^{44}Ca	^{263}122	176.7790	4.79×10^{21}	3.91×10^{-20}	1.87×10^{2}	−2.4324
	^{46}Ca	^{261}122	182.9210	4.95×10^{21}	2.28×10^{-18}	1.13×10^{4}	−4.2126
	^{48}Ca	^{259}122	188.3950	5.1×10^{21}	1.79×10^{-16}	9.12×10^{5}	−6.11979
	^{12}C	^{296}122	49.2600	1.33×10^{21}	1.07×10^{-20}	1.42×10^{1}	−1.31257
	^{14}C	^{294}122	50.1300	1.36×10^{21}	7.92×10^{-29}	1.08×10^{-7}	6.808576
	^{14}N	^{294}122	52.2570	1.41×10^{21}	2.35×10^{-26}	3.33×10^{-5}	4.317715
	^{20}Ne	^{288}122	80.5120	2.18×10^{21}	1.88×10^{-25}	4.10×10^{-4}	3.226809
	^{22}Ne	^{286}122	85.4950	2.31×10^{21}	2.11×10^{-22}	4.88×10^{-1}	0.151704
^{308}122	^{24}Ne	^{284}122	85.0780	2.3×10^{21}	3.91×10^{-22}	9.01×10^{-1}	−0.11467
	^{28}Si	^{280}122	115.7230	3.13×10^{21}	1.96×10^{-25}	6.15×10^{-4}	3.051528
	^{30}Si	^{278}122	122.9930	3.33×10^{21}	4.61×10^{-22}	0.154×10^{1}	−0.34604
	^{32}Si	^{276}122	126.6580	3.43×10^{21}	3.58×10^{-20}	1.23×10^{2}	−2.2496
	^{34}Si	^{274}122	126.3320	3.42×10^{21}	6.75×10^{-20}	2.31×10^{2}	−2.52302
	^{36}Ar	^{272}122	144.0720	3.9×10^{21}	1.34×10^{-26}	5.23×10^{-5}	4.121359
	^{38}Ar	^{270}122	154.9650	4.2×10^{21}	9.88×10^{-23}	4.14×10^{-1}	0.222669
	^{40}Ar	^{268}122	159.5660	4.32×10^{21}	3.88×10^{-20}	1.68×10^{2}	−2.3848
	^{42}Ar	^{266}122	164.2470	4.45×10^{21}	9.45×10^{-19}	4.20×10^{3}	−3.78361
	^{44}Ar	^{264}122	166.1970	4.5×10^{21}	5.73×10^{-18}	2.58×10^{4}	−4.57162
	^{40}Ca	^{268}122	158.3360	4.29×10^{21}	5.9×10^{-27}	2.53×10^{-5}	4.436773
	^{42}Ca	^{266}122	168.5070	4.56×10^{21}	2.38×10^{-23}	1.09×10^{-1}	0.804158
	^{44}Ca	^{264}122	176.5190	4.78×10^{21}	3.7×10^{-20}	1.77×10^{2}	−2.40724
	^{46}Ca	^{262}122	182.8840	4.95×10^{21}	2.44×10^{-18}	1.21×10^{4}	−4.24201
	^{48}Ca	^{260}122	188.3030	5.1×10^{21}	1.87×10^{-16}	9.52×10^{5}	−6.13872
	^{12}C	^{297}122	49.6300	1.34×10^{21}	2.6×10^{-20}	3.49×10^{1}	−1.70283
	^{14}C	^{295}122	50.9400	1.38×10^{21}	3.71×10^{-28}	5.12×10^{-7}	6.130767
	^{14}N	^{295}122	53.7170	1.45×10^{21}	5.83×10^{-25}	8.48×10^{-4}	2.911618
	^{20}Ne	^{289}122	80.9320	2.19×10^{21}	3.12×10^{-25}	6.84×10^{-4}	3.005138
	^{22}Ne	^{287}122	86.1250	2.33×10^{21}	5.9×10^{-22}	0.138×10^{1}	−0.29874
^{309}122	^{24}Ne	^{285}122	86.6950	2.35×10^{21}	7.12×10^{-21}	1.67×10^{1}	−1.383
	^{28}Si	^{281}122	115.9430	3.14×10^{21}	3.37×10^{-25}	1.06×10^{-3}	2.815154
	^{30}Si	^{279}122	123.4030	3.34×10^{21}	7.08×10^{-22}	0.236×10^{1}	−0.53357
	^{32}Si	^{277}122	127.4250	3.45×10^{21}	9.4×10^{-20}	3.24×10^{2}	−2.67067
	^{34}Si	^{275}122	126.9240	3.44×10^{21}	1.46×10^{-19}	5.02×10^{2}	−2.86061
	^{36}Ar	^{273}122	143.7120	3.89×10^{21}	1.15×10^{-26}	4.48×10^{-5}	4.188599
	^{38}Ar	^{271}122	154.3050	4.18×10^{21}	6.03×10^{-23}	2.52×10^{-1}	0.438656
	^{40}Ar	^{269}122	160.7000	4.35×10^{21}	7.52×10^{-20}	3.27×10^{2}	−2.67447
	^{42}Ar	^{267}122	164.1390	4.44×10^{21}	9.61×10^{-19}	4.27×10^{3}	−3.79061
	^{44}Ar	^{265}122	166.8840	4.52×10^{21}	9.42×10^{-18}	4.26×10^{4}	−4.78901
	^{40}Ca	^{269}122	157.4160	4.26×10^{21}	3.59×10^{-27}	1.53×10^{-5}	4.654801
	^{42}Ca	^{267}122	167.7270	4.54×10^{21}	1.32×10^{-23}	5.97×10^{-2}	1.063913
	^{44}Ca	^{265}122	176.9380	4.79×10^{21}	4.97×10^{-20}	2.38×10^{2}	−2.53637
	^{46}Ca	^{263}122	183.0760	4.96×10^{21}	3.00×10^{-18}	1.49×10^{4}	−4.33175
	^{48}Ca	^{261}122	188.6300	5.11×10^{21}	2.72×10^{-16}	1.39×10^{6}	−6.30323
	^{12}C	^{298}122	49.4900	1.34×10^{21}	2.03×10^{-20}	2.72×10^{1}	−1.59428
	^{14}C	^{296}122	51.1600	1.39×10^{21}	6.06×10^{-28}	8.39×10^{-7}	5.91617
	^{14}N	^{296}122	52.5770	1.42×10^{21}	1.02×10^{-25}	1.46×10^{-4}	3.677131
	^{20}Ne	^{290}122	81.2220	2.2×10^{21}	4.54×10^{-25}	9.98×10^{-4}	2.840811
	^{22}Ne	^{288}122	86.4150	2.34×10^{21}	1.05×10^{-21}	0.246×10^{1}	−0.55053
	^{24}Ne	^{286}122	88.3420	2.39×10^{21}	6.84×10^{-20}	1.64×10^{2}	−2.37369
	^{28}Si	^{282}122	115.7730	3.13×10^{21}	2.81×10^{-25}	8.82×10^{-4}	2.894855
^{310}122	^{30}Si	^{280}122	123.5830	3.35×10^{21}	8.97×10^{-22}	0.300×10^{1}	−0.6374
	^{32}Si	^{278}122	127.5610	3.45×10^{21}	1.24×10^{-19}	4.28×10^{2}	−2.79095
	^{34}Si	^{276}122	127.4540	3.45×10^{21}	3.18×10^{-19}	1.10×10^{3}	−3.19979
	^{36}Ar	^{274}122	143.0420	3.87×10^{21}	8.14×10^{-27}	3.15×10^{-5}	4.341648
	^{38}Ar	^{272}122	153.4750	4.16×10^{21}	3.24×10^{-23}	1.35×10^{-1}	0.710629

TABLE II. (*Continued.*)

Parent nuclei	Emitted cluster	Daughter nuclei	Q value(MeV)	Penetrability P	Decay constant λ	$\log_{10}T_{1/2}$	Parent nuclei
	^{40}Ar	^{270}122	160.2100	4.34×10^{21}	6.25×10^{-20}	2.71×10^{2}	−2.5931
	^{42}Ar	^{268}122	163.8690	4.44×10^{21}	8.92×10^{-19}	3.96×10^{3}	−3.75732
	^{44}Ar	^{266}122	167.4170	4.53×10^{21}	1.42×10^{-17}	6.44×10^{4}	−4.96906
	^{40}Ca	^{270}122	156.2660	4.23×10^{21}	1.91×10^{-27}	8.09×10^{-6}	4.932028
	^{42}Ca	^{268}122	166.9570	4.52×10^{21}	7.54×10^{-24}	3.41×10^{-2}	1.30761
	^{44}Ca	^{266}122	176.3480	4.77×10^{21}	3.95×10^{-20}	1.89×10^{2}	−2.43543
	^{46}Ca	^{264}122	183.1060	4.96×10^{21}	3.34×10^{-18}	1.66×10^{4}	−4.37892
	^{48}Ca	^{262}122	188.8830	5.11×10^{21}	3.79×10^{-16}	1.94×10^{6}	−6.44697
	^{12}C	^{299}122	49.3100	1.34×10^{21}	1.46×10^{-20}	1.95×10^{1}	−1.45061
	^{14}C	^{297}122	51.3700	1.39×10^{21}	9.81×10^{-28}	1.36×10^{-6}	5.704987
	^{14}N	^{297}122	53.4570	1.45×10^{21}	4.47×10^{-25}	6.48×10^{-4}	3.028727
	^{20}Ne	^{291}122	81.1920	2.2×10^{21}	4.71×10^{-25}	1.04×10^{-3}	2.824779
	^{22}Ne	^{289}122	86.6750	2.35×10^{21}	1.88×10^{-21}	0.441×10^{1}	−0.80441
	^{24}Ne	^{287}122	88.8120	2.4×10^{21}	1.1×10^{-19}	2.65×10^{2}	−2.583
	^{28}Si	^{283}122	115.5630	3.13×10^{21}	2.22×10^{-25}	6.93×10^{-4}	2.999274
^{311}122	^{30}Si	^{281}122	146.8030	3.97×10^{21}	1.92×10^{-12}	7.63×10^{9}	−10.0422
	^{32}Si	^{279}122	127.8110	3.46×10^{21}	1.91×10^{-19}	6.61×10^{2}	−2.98039
	^{34}Si	^{277}122	128.0610	3.47×10^{21}	9.08×10^{-19}	3.15×10^{3}	−3.6578
	^{36}Ar	^{275}122	141.9320	3.84×10^{21}	4.38×10^{-27}	1.68×10^{-5}	4.613658
	^{38}Ar	^{273}122	152.9550	4.14×10^{21}	2.31×10^{-23}	9.56×10^{-2}	0.859796
	^{40}Ar	^{271}122	159.3900	4.32×10^{21}	4.38×10^{-20}	1.89×10^{2}	−2.43691
	^{42}Ar	^{269}122	164.8430	4.46×10^{21}	1.68×10^{-18}	7.49×10^{3}	−4.03434
	^{44}Ar	^{267}122	167.1490	4.53×10^{21}	1.31×10^{-17}	5.93×10^{4}	−4.93269
	^{40}Ca	^{271}122	155.3460	4.21×10^{21}	1.18×10^{-27}	4.97×10^{-6}	5.144005
	^{42}Ca	^{269}122	165.8770	4.49×10^{21}	3.44×10^{-24}	1.54×10^{-2}	1.65157
	^{44}Ca	^{267}122	175.4080	4.75×10^{21}	2.63×10^{-20}	1.25×10^{2}	−2.25625
	^{46}Ca	^{265}122	183.3650	4.96×10^{21}	4.28×10^{-18}	2.13×10^{4}	−4.48764
	^{48}Ca	^{263}122	188.9150	5.12×10^{21}	4.40×10^{-16}	2.25×10^{6}	−6.51241
	^{12}C	^{300}122	48.8500	1.32×10^{21}	6×10^{-21}	0.793×10^{1}	−1.05919
	^{14}C	^{298}122	51.2500	1.39×10^{21}	8.29×10^{-28}	1.15×10^{-6}	5.779013
	^{14}N	^{298}122	51.9270	1.41×10^{21}	1.39×10^{-26}	1.96×10^{-5}	4.547803
	^{20}Ne	^{292}122	80.8320	2.19×10^{21}	3.45×10^{-25}	7.55×10^{-4}	2.962102
	^{22}Ne	^{290}122	86.9850	2.36×10^{21}	4.26×10^{-21}	1.00×10^{1}	−1.16119
	^{24}Ne	^{288}122	89.1220	2.41×10^{21}	1.55×10^{-19}	3.73×10^{2}	−2.73218
	^{28}Si	^{284}122	114.9930	3.11×10^{21}	1.02×10^{-25}	3.19×10^{-4}	3.336952
^{312}122	^{30}Si	^{282}122	123.4930	3.34×10^{21}	9.81×10^{-22}	0.328×10^{1}	−0.67592
	^{32}Si	^{280}122	128.0110	3.47×10^{21}	2.84×10^{-19}	9.86×10^{2}	−3.15362
	^{34}Si	^{278}122	128.2170	3.47×10^{21}	1.47×10^{-18}	5.09×10^{3}	−3.86671
	^{36}Ar	^{276}122	141.3020	3.83×10^{21}	9.64×10^{-28}	3.69×10^{-6}	5.273239
	^{38}Ar	^{274}122	152.3050	4.12×10^{21}	1.49×10^{-23}	6.13×10^{-2}	1.052494
	^{40}Ar	^{272}122	158.5800	4.29×10^{21}	3.1×10^{-20}	1.33×10^{2}	−2.28429
	^{42}Ar	^{270}122	164.3730	4.45×10^{21}	1.38×10^{-18}	6.16×10^{3}	−3.94965
	^{44}Ar	^{268}122	166.8990	4.52×10^{21}	1.22×10^{-17}	5.51×10^{4}	−4.90109
	^{40}Ca	^{272}122	154.3260	4.18×10^{21}	6.91×10^{-28}	2.89×10^{-6}	5.379844
	^{42}Ca	^{270}122	164.7470	4.46×10^{21}	1.56×10^{-24}	2.89×10^{-6}	1.996791
	^{44}Ca	^{268}122	174.6580	4.73×10^{21}	1.93×10^{-20}	9.15×10^{1}	−2.12119
	^{46}Ca	^{266}122	182.7950	4.95×10^{21}	3.31×10^{-18}	1.64×10^{4}	−4.37401
	^{48}Ca	^{264}122	188.9650	5.12×10^{21}	5.21×10^{-16}	2.66×10^{6}	−6.58556
	^{12}C	^{301}122	47.9200	1.3×10^{21}	1.09×10^{-21}	0.141×10^{1}	−0.30957
	^{14}C	^{299}122	51.2500	1.39×10^{21}	8.89×10^{-28}	1.23×10^{-6}	5.749116
	^{14}N	^{299}122	52.6770	1.43×10^{21}	1.62×10^{-25}	2.31×10^{-4}	3.476317
	^{20}Ne	^{293}122	80.6920	2.18×10^{21}	3.19×10^{-25}	6.96×10^{-4}	2.997325
	^{22}Ne	^{291}122	87.1350	2.36×10^{21}	9.36×10^{-21}	2.21×10^{1}	−1.50396
	^{24}Ne	^{289}122	89.5620	2.43×10^{21}	2.46×10^{-19}	5.96×10^{2}	−2.93501
^{313}122	^{28}Si	^{285}122	114.4530	3.1×10^{21}	5.39×10^{-26}	1.67×10^{-4}	3.616912
	^{30}Si	^{283}122	123.4630	3.34×10^{21}	1.04×10^{-21}	0.347×10^{1}	−0.70058
	^{32}Si	^{281}122	128.2510	3.47×10^{21}	4.68×10^{-19}	1.63×10^{3}	−3.37104

TABLE II. (*Continued.*)

Parent nuclei	Emitted cluster	Daughter nuclei	Q value(MeV)	Penetrability P	Decay constant λ	$\log_{10}T_{1/2}$	Parent nuclei
	^{34}Si	^{279}122	128.6470	3.48×10^{21}	4.48×10^{-18}	1.56×10^{4}	−4.35275
	^{36}Ar	^{277}122	140.6620	3.81×10^{21}	4.13×10^{-28}	1.57×10^{-6}	5.643293
	^{38}Ar	^{275}122	151.3750	4.1×10^{21}	7.76×10^{-24}	3.18×10^{-2}	1.33764
	^{40}Ar	^{273}122	158.2400	4.28×10^{21}	2.79×10^{-20}	1.20×10^{2}	−2.2378
	^{42}Ar	^{271}122	163.7330	4.43×10^{21}	1.04×10^{-18}	4.60×10^{3}	−3.82299
	^{44}Ar	^{269}122	168.0530	4.55×10^{21}	2.74×10^{-17}	1.25×10^{5}	−5.25536
	^{40}Ca	^{273}122	153.0760	4.14×10^{21}	1.12×10^{-28}	4.66×10^{-7}	6.172113
	^{42}Ca	^{271}122	164.0070	4.44×10^{21}	9.8×10^{-25}	4.35×10^{-3}	2.201385
	^{44}Ca	^{269}122	173.7580	4.7×10^{21}	1.32×10^{-20}	6.23×10^{1}	−1.95411
	^{46}Ca	^{267}122	182.0350	4.93×10^{21}	2.29×10^{-18}	1.13×10^{4}	−4.21167
	^{48}Ca	^{265}122	189.4040	5.13×10^{21}	8.83×10^{-16}	4.53×10^{6}	−6.81602
	^{12}C	^{302}122	47.1500	1.28×10^{21}	2.97×10^{-22}	3.80×10^{-1}	0.260678
	^{14}C	^{300}122	50.7300	1.37×10^{21}	3.49×10^{-28}	4.80×10^{-7}	6.158867
	^{14}N	^{300}122	49.9370	1.35×10^{21}	2.67×10^{-28}	3.62×10^{-7}	6.281974
	^{20}Ne	^{294}122	79.9020	2.16×10^{21}	1.5×10^{-25}	3.25×10^{-4}	3.327909
	^{22}Ne	^{292}122	86.7150	2.35×10^{21}	2.89×10^{-21}	0.679×10^{1}	−0.99161
	^{24}Ne	^{290}122	89.8120	2.43×10^{21}	3.3×10^{-19}	8.01×10^{2}	−3.06371
^{314}122	^{28}Si	^{286}122	113.5230	3.07×10^{21}	1.85×10^{-26}	5.7×10^{-5}	4.084265
	^{30}Si	^{284}122	122.8330	3.33×10^{21}	6.58×10^{-22}	0.219×10^{1}	−0.4997
	^{32}Si	^{282}122	128.0410	3.47×10^{21}	3.86×10^{-19}	1.34×10^{3}	−3.28639
	^{34}Si	^{280}122	128.7870	3.49×10^{21}	5.17×10^{-18}	1.80×10^{4}	−4.41547
	^{36}Ar	^{278}122	139.7520	3.78×10^{21}	1.45×10^{-28}	0.54×10^{-7}	6.101623
	^{38}Ar	^{276}122	150.6850	4.08×10^{21}	4.96×10^{-24}	2.03×10^{-2}	1.533564
	^{40}Ar	^{274}122	157.5300	4.27×10^{21}	2.08×10^{-20}	8.89×10^{1}	−2.10881
	^{42}Ar	^{272}122	162.8630	4.41×10^{21}	6.86×10^{-19}	3.03×10^{3}	−3.64088
	^{44}Ar	^{270}122	167.5230	4.54×10^{21}	2.13×10^{-17}	9.65×10^{4}	−5.14425
	^{40}Ca	^{274}122	152.0060	4.12×10^{21}	2.78×10^{-29}	1.14×10^{-7}	6.781859
	^{42}Ca	^{272}122	162.9270	4.41×10^{21}	4.84×10^{-25}	2.14×10^{-3}	2.510313
	^{44}Ca	^{270}122	172.5680	4.67×10^{21}	7.88×10^{-21}	3.68×10^{1}	−1.72571
	^{46}Ca	^{271}122	181.2250	4.91×10^{21}	1.54×10^{-18}	7.57×10^{3}	−4.03888
	^{48}Ca	^{266}122	188.7740	5.11×10^{21}	5.66×10^{-16}	2.89×10^{6}	−6.62145

TABLE III. Branching ratio of alpha decay with respect to the spontaneous fission, ternary fission, and cluster decay for different isotopes of superheavy nuclei $Z = 122$.

$\lambda\alpha$/(SF)	$\lambda\alpha$/(TF)	$\lambda_\alpha/\lambda_{CR}$					
		^{12}C	^{14}N	^{20}Ne	^{30}Si	^{40}Ar	^{40}Ca
1.72×10^{7}	2.45×10^{11}	4.59×10^{3}	2.01×10^{8}	1.84×10^{8}	4.39×10^{4}	3.37×10^{2}	1.53×10^{9}
2.27×10^{3}	1.09×10^{12}	2.94×10^{3}	1.26×10^{9}	1.02×10^{8}	2.72×10^{4}	2.49×10^{2}	1.65×10^{9}
3.85×10^{3}	6.42×10^{7}	6.90×10^{2}	2.84×10^{7}	3.52×10^{7}	1.02×10^{4}	7.37×10^{1}	1.57×10^{9}
1.30×10^{4}	3.07×10^{8}	4.99×10^{2}	9.32×10^{7}	9.32×10^{7}	4.52×10^{3}	5.00×10^{1}	1.68×10^{9}
3.07×10^{4}	2.89×10^{7}	3.82×10^{2}	1.15×10^{7}	7.21×10^{6}	9.8×10^{-7}	3.95×10^{1}	3.32×10^{-3}
3.77×10^{37}	3.79×10^{8}	5.08×10^{2}	2.06×10^{8}	5.34×10^{6}	1.23×10^{3}	3.03×10^{1}	1.40×10^{9}
1.99×10^{5}	3.23×10^{7}	1.51×10^{3}	9.23×10^{6}	3.06×10^{6}	6.14×10^{2}	1.78×10^{1}	4.58×10^{9}
5.01×10^{5}	2.88×10^{10}	2.92×10^{3}	3.07×10^{9}	3.41×10^{6}	5.07×10^{2}	1.25×10^{1}	9.70×10^{9}

TABLE IV. The computed logarithmic half-life values for various decay modes of superheavy nuclei $Z = 122$.

Isotope	Spontaneous fission half-life (yr)	Ternary fission half-life (yr)	Cluster radioactivity (yr)						α decay (yr)
			^{12}C	^{14}N	^{20}Ne	^{30}Si	^{40}Ar	^{40}Ca	
^{307}122	1.69×10^{2}	2.40×10^{6}	4.50×10^{-2}	1.97×10^{3}	1.81×10^{3}	4.30×10^{-1}	3.31×10^{-3}	1.50×10^{4}	9.80×10^{-6}
^{308}122	3.76×10^{-2}	1.80×10^{7}	4.87×10^{-2}	2.08×10^{4}	1.69×10^{3}	4.51×10^{-1}	4.12×10^{-3}	2.73×10^{4}	1.66×10^{-5}
^{309}122	1.11×10^{-1}	1.84×10^{3}	1.98×10^{-2}	8.16×10^{2}	1.01×10^{3}	2.93×10^{-1}	2.12×10^{-3}	4.52×10^{4}	2.87×10^{-5}
^{310}122	6.63×10^{-1}	1.56×10^{4}	2.55×10^{-2}	4.75×10^{3}	4.75×10^{3}	2.30×10^{-1}	2.55×10^{-3}	8.55×10^{4}	5.10×10^{-5}
^{311}122	2.84×10^{0}	2.68×10^{3}	3.54×10^{-2}	1.07×10^{3}	6.68×10^{2}	9.07×10^{-11}	3.66×10^{-3}	3.07×10^{-7}	9.27×10^{-5}
^{312}122	6.48×10^{33}	6.51×10^{4}	8.73×10^{-2}	3.53×10^{4}	9.16×10^{2}	2.11×10^{-1}	5.20×10^{-3}	2.40×10^{5}	1.72×10^{-4}
^{313}122	6.45×10^{1}	1.05×10^{4}	4.90×10^{-1}	2.99×10^{3}	9.94×10^{2}	1.99×10^{-1}	5.78×10^{-3}	1.49×10^{6}	3.24×10^{-4}
^{314}122	3.12×10^{2}	1.80×10^{7}	1.82×10^{0}	1.91×10^{6}	2.13×10^{3}	3.16×10^{-1}	7.78×10^{-3}	6.05×10^{6}	6.24×10^{-4}

[1] A. Diaz-Torres, G. G. Adamian, N. V. Antonenko, and W. Scheid, Phys. Rev. C **64**, 024604 (2001).
[2] N. V. Antonenko, E. A. Cherepanov, A. K. Nasirov, V. P. Permjakov, and V. V. Volkov, Phys. Rev. C **51**, 2635 (1995).
[3] G. G. Adamian, N. V. Antonenko, and W. Scheid, Nucl. Phys. A **618**, 176 (1997).
[4] G. G. Adamian, N.V. Antonenko, S. E Ivanova, and W. Scheid, Nucl. Phys. A **646**, 29 (1999).
[5] G. G. Adamian, N. V. Antonenko, W. Scheid, and V. V. Volkov, Nucl. Phys. A **633**, 409 (1998).
[6] G. G. Adamian, N. V. Antonenko, and W. Scheid, Nucl. Phys. A **678**, 24 (2000).
[7] G. G. Adamian, N. V. Antonenko, and W. Scheid, Phys. Rev. C **69**, 044601 (2004).
[8] Sh. A. Kalandarov, G. G. Adamian, N. V. Antonenko, and W. Scheid, Phys. Rev. C **83**, 054611 (2011).
[9] V. I. Zagrebaev, Phys. Rev. C **64**, 034606 (2001).
[10] V. I. Zagrebaev, B. Fornal, S. Leoni, and W. Greiner, Phys. Rev. C **89**, 054608 (2014).
[11] V. I. Zagrebaev, Phys. Rev. C **78**, 047602 (2008).
[12] V. I. Zagrebaev and W. Greiner, Phys. Rev. C **83**, 044618 (2011).
[13] V. I. Zagrebaev, A. V. Karpov, I. N. Mishustin, and W. Greiner, Phys. Rev. C **84**, 044617 (2011).
[14] A. Marinov, I. Rodushkin, D. Kolb, A. Pape, Y. Kashiv, R. Brandt, R. V. Gentry, and H. W. Miller, Int. J. Mod. Phys. E **19**, 131 (2010).
[15] Y. T. Oganessian, J. Phys. G: Nucl. Part. Phys. **34**, R165 (2007).
[16] M. G. Itkis, E. Vardaci, I. M. Itkis, G. N. Knyazheva, and E. M. Kozulin, Nucl. Phys. A **944**, 204 (2015).
[17] W. Q. Shen, J. Albinski, A. Gobbi, S. Gralla *et al.*, Phys. Rev. C **36**, 115 (1987).
[18] T. Cap, K. Siwek-Wilczynska, and J. Wilczynski, Phys. Lett. B **736**, 478 (2014).
[19] R. K. Choudhury and Y. K. Gupta, Phys. Lett. B **731**, 168 (2014).
[20] V. L. Litnevsky, G. I. Kosenko, and F. A. Ivanyuk, Phys. Rev. C **93**, 064606 (2016).
[21] W. J. Swiatecki, K. Siwek-Wilczyńska, and J. Wilczyński, Phys. Rev. C **71**, 014602 (2005).
[22] H. C. Manjunatha and K. N. Sridhar, Eur. Phys. J. A **53**, 97 (2017).
[23] H. C. Manjunatha and K. N. Sridhar, Eur. Phys. J. A **53**, 196 (2017).
[24] H. C. Manjunatha and K. N. Sridhar, Nucl. Phys. A **962**, 7 (2017).
[25] H. C. Manjunatha and N. Sowmya, Nucl. Phys. A **969**, 68 (2018).
[26] H. C. Manjunatha, Int. J. Mod. Phys. E **25**, 1650100 (2016).
[27] H. C. Manjunatha, Int. J. Mod. Phys. E **25**, 1650074 (2016).
[28] H. C. Manjunatha, Nucl. Phys. A **945**, 42 (2016).
[29] J. Blocki, J. Randrup, W. J. Swiatecki, and C. F. Tsang, Ann. Phys. (N.Y.) **105**, 427 (1977).
[30] L. Zheng, G. L. Zhang, J. C. Yang, and W. W. Qu, Nucl. Phys. A **915**, 70 (2013).
[31] G. L. Zhang, H. B. Zheng, and W. W. Qu, Eur. Phys. J. A **49**, 10 (2013).
[32] J. Blocki and W. J. Swiatecki, Ann. Phys. (N.Y.) **132**, 53 (1981).
[33] C. Y. Wong, Phys. Lett. B **42**, 186 (1972).
[34] W. Loveland, Phys. Rev. C **75**, 069801 (2007).
[35] V. Zagrebaev and W. Greiner, Phys. Rev. C **78**, 034610 (2008).
[36] P. Armbruster, Rep. Prog. Phys. **62**, 465 (1999).
[37] S. A. Kalandarov, G. G. Adamian, N. V. Antonenko, and W. Scheid, Phys. Rev. C **82**, 044603 (2010).
[38] Z. H. Liu and J. D. Bao, Phys. Rev. C **81**, 044606 (2010).
[39] J. D. Jackson, Can. J. Phys. **34**, 767 (1956).
[40] R. Vandenbosch and J. R. Huizenga, *Nuclear Fission* (Academic, New York, 1973).
[41] W. Loveland, Phys. Rev. C **76**, 014612 (2007).
[42] V. Y. Denisov, Phys. Lett. B **526**, 315 (2002).
[43] H. Koura, T. Tachibana, M. Uno, and M. Yamada, Prog. Theor. Phys. **113**, 305 (2005).
[44] M. Kowal, P. Jachimowicz, and A. Sobiczewski, Phys. Rev. C **82**, 014303 (2010).
[45] H. C. Manjunatha, B. M. Chandrika, and L. Seenappa, Mod. Phys. Lett. A **31**, 1650162 (2016).